Supplementary Material

7 Supplementary Figures, S1-S7 with legends

Supplementary Figure 1

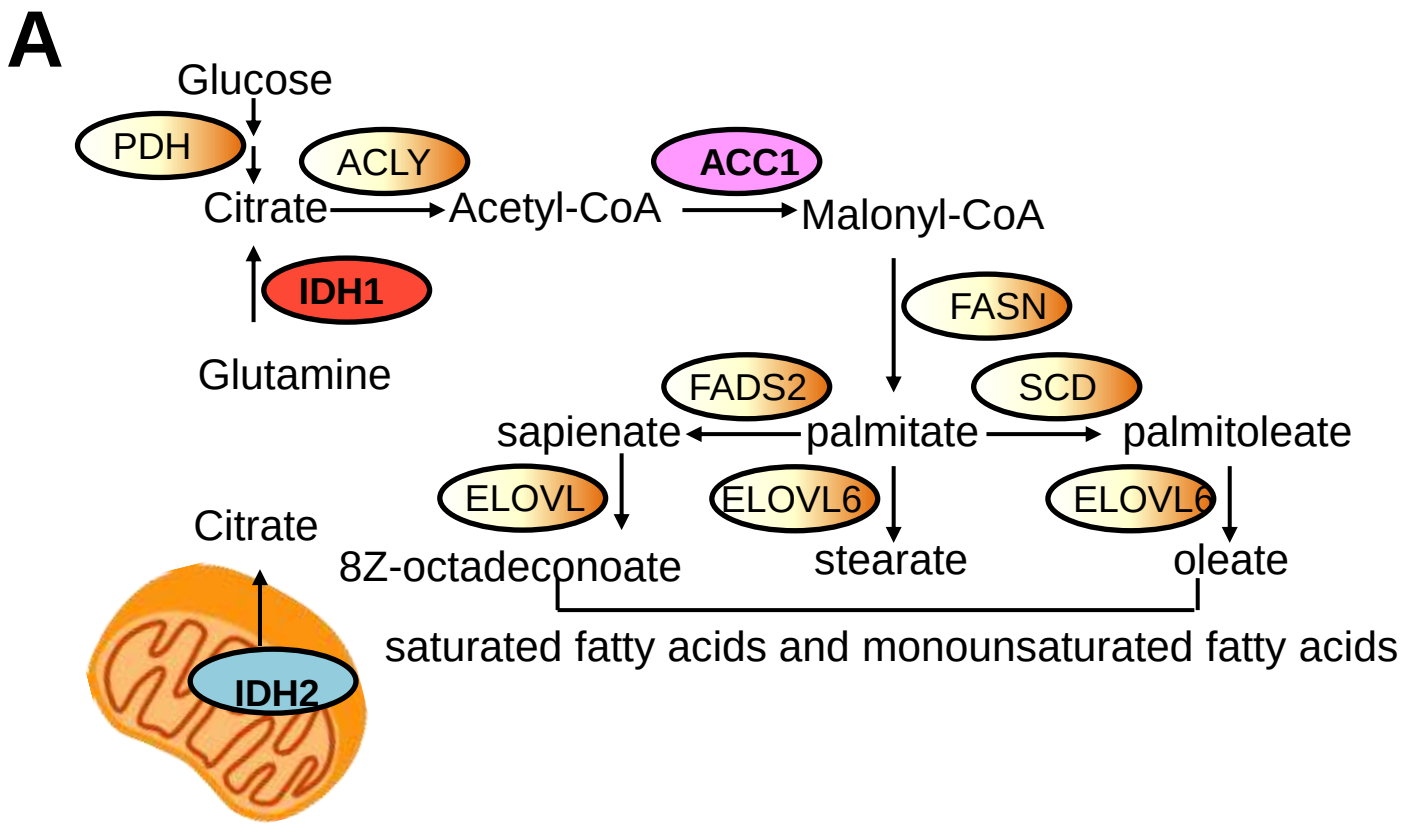

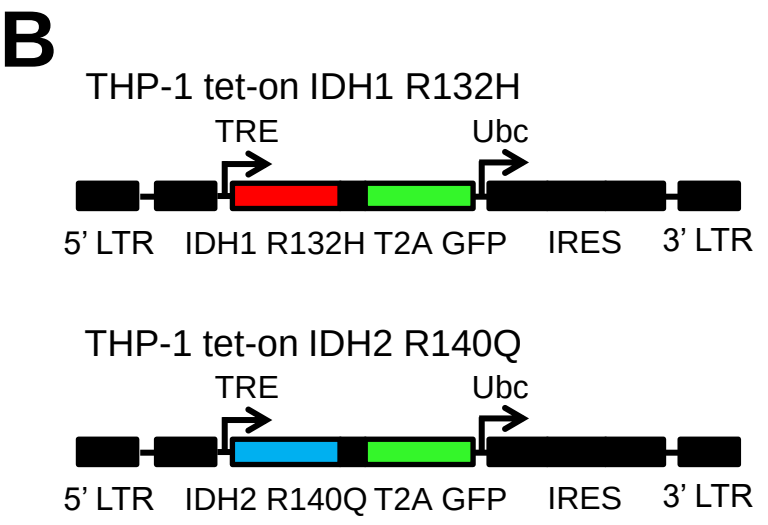

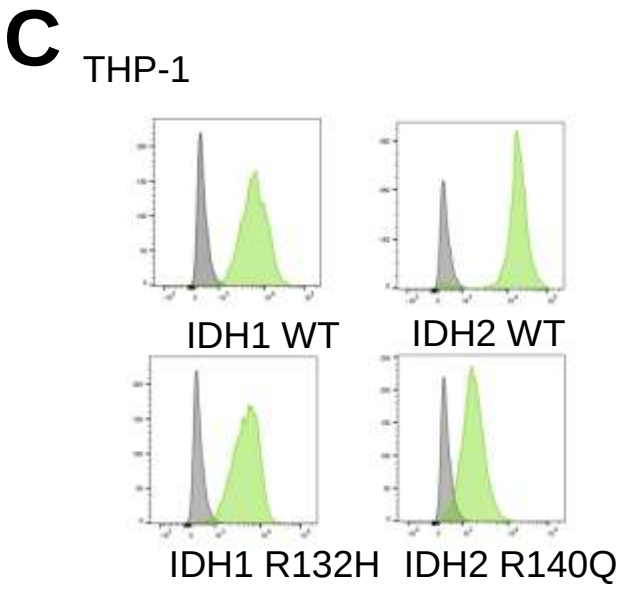

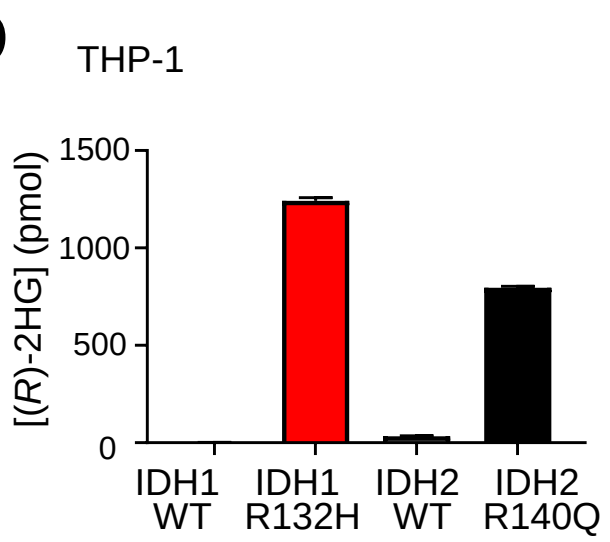

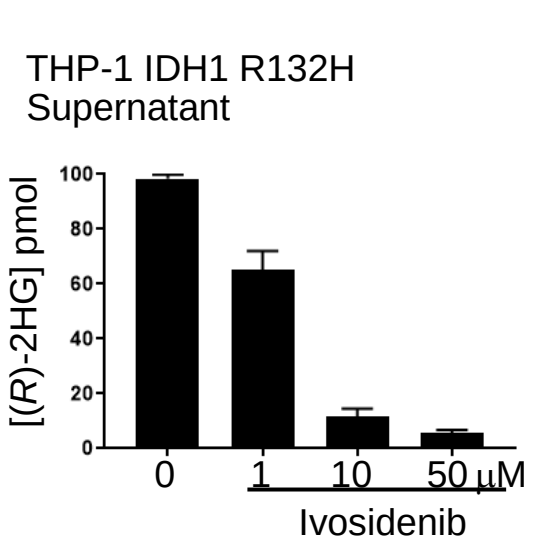

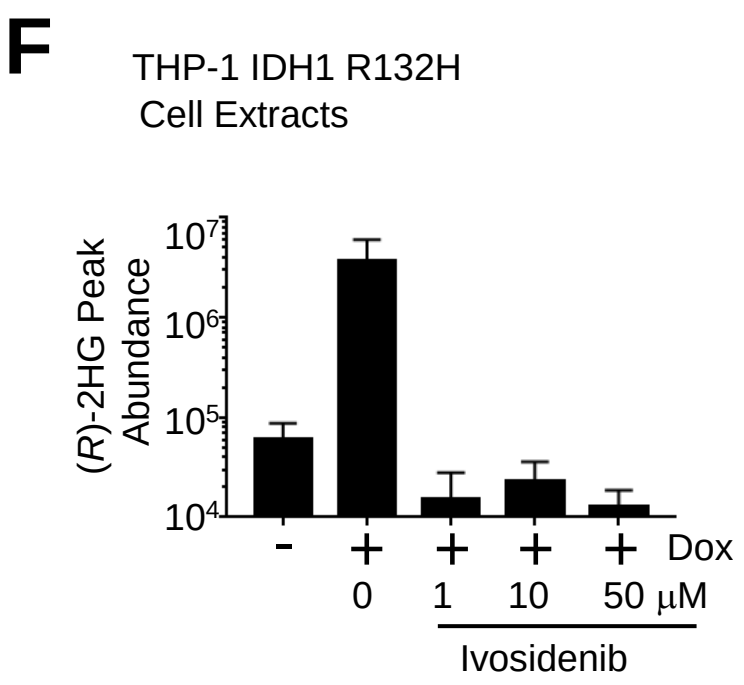

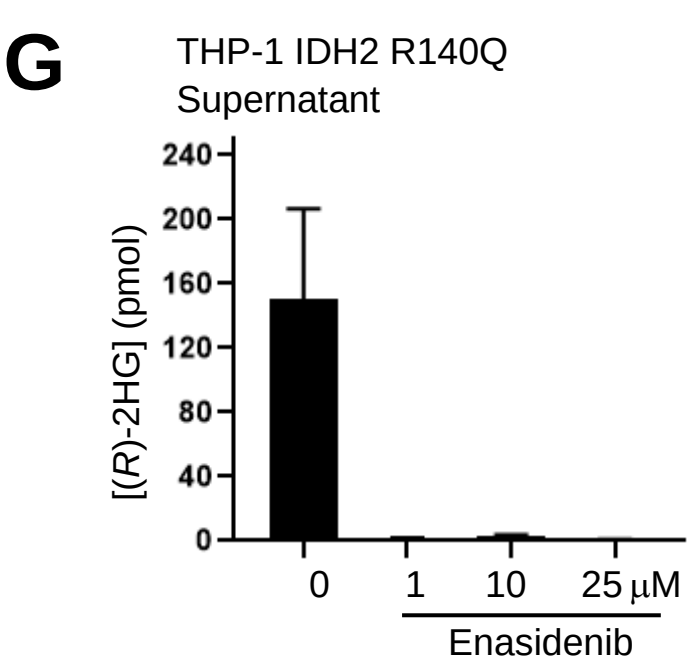

Supplementary Figure 1 (continued)

Supplementary Figure 1. Metabolic differences between IDH1 and IDH2 mutations. A. Pathway of de novo lipid synthesis in mammalian cells. IDH1 has a critical role upstream of ACC1 in supply of carbon in the form of acetyl CoA derived from isocitrate. IDH2, located in the mitochondria can also supply isocitrate (via ACLY) to the cytoplasm from the Kreb's cycle for macromolecular synthesis. ACC1 is a cytoplasmic isoform regulating fatty acid synthesis. Fatty acid synthase (FASN) uses malonyl-CoA and acetyl-CoA to catalyse subsequent successive reactions to form fatty acids and subsequent elongation and desaturation reactions via fatty acid elongases (ELOVL1-7) and fatty acid desaturases (SCD, SCD5) respectively produce a milieu of monounsaturated and saturated fatty acids. Both elongation and desaturation reactions are highly dependent on sufficient reduced NADPH in cytosol. **B.** Doxycycline-inducible lentiviral plasmids used to construct isogenic cell-lines with self-cleaving peptide separating IDH protein and eGFP. **C**. Induction of eGFP in THP-1 after 72 hours of doxycycline (1 μg/ml). **D.** Quantitation of (*R*)-2HG measured in cell culture media 72 h after doxycycline addition. Error bars represent standard deviation of 6 replicates in a typical experiment. **E.** (*R*)-2HG levels measured in supernatant after increasing concentrations of ivosidenib as shown in THP-1 IDH1 R132H (+dox) cells. **F**. (*R*)-2HG levels measured from cell pellets after increasing concentrations of ivosidenib in THP-1 IDH1 R132H (+ dox) cells. **G**. (*R*)-2HG levels measured in supernatant after increasing concentrations of enasidenib in doxycycline-induced THP-1 IDH2 R140Q-T2A-eGFP (+ dox) cells. Error bars represent standard deviation of technical replicates from representative experiments.

Supplementary Figure 2

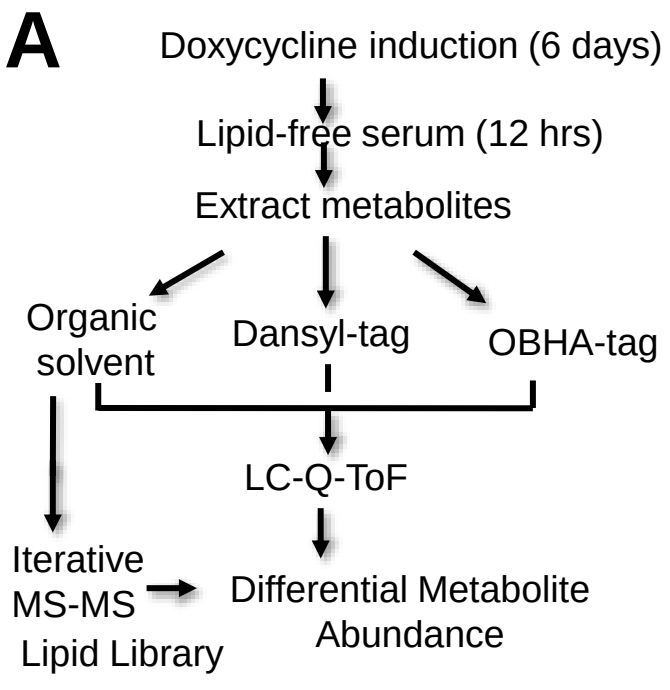

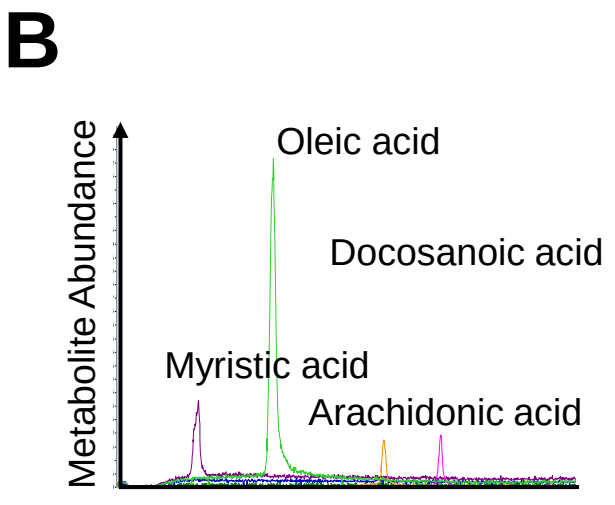

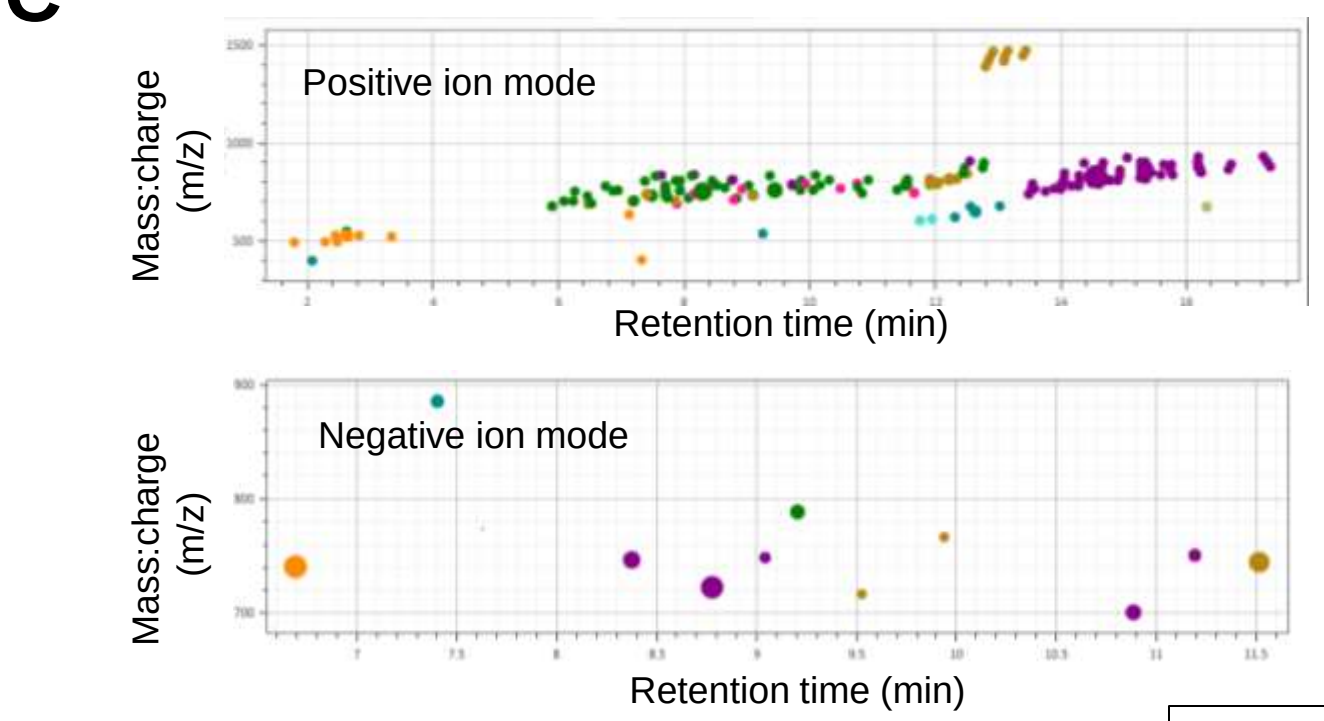

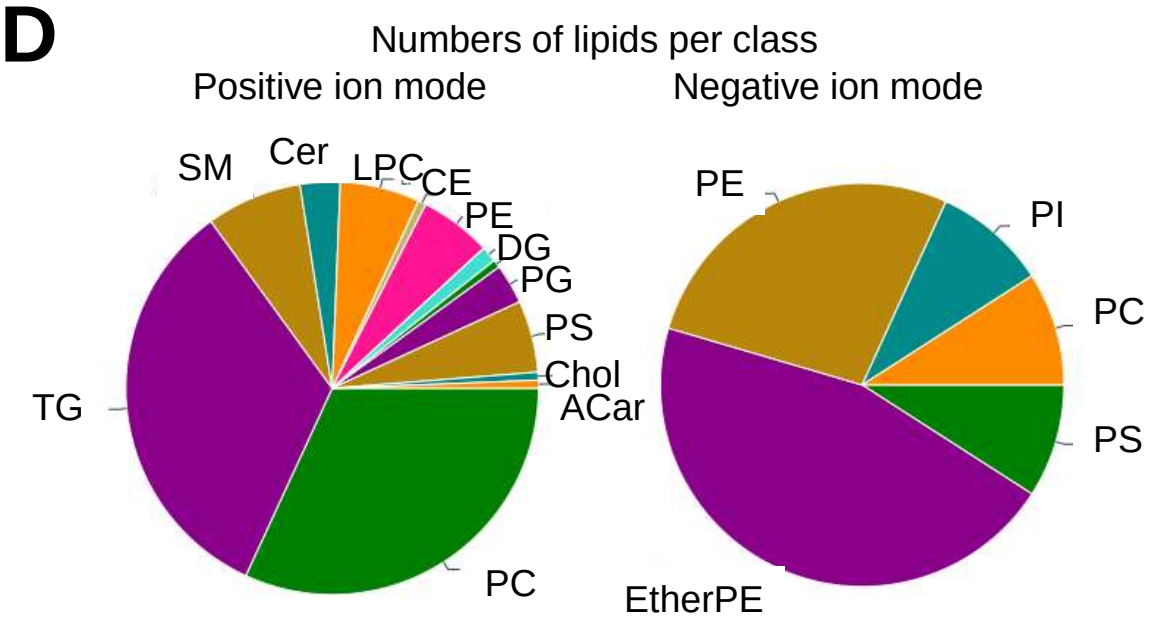

Supplementary Figure 2. Detection of lipidomic changes between mutant *IDH1* and *IDH2* AML. A. Schematic for metabolomics studies in isogenic AML cell-lines after culturing in lipid-free serum containing media. **B**. Method validation showing examples of peak abundance for commonly detected lipids myristic acid, docosanoic acid, arachidonic acid and oleic acid. **C**. Graphs showing all lipid species detected in THP-1 cells and identified by iterative MS-MS. Y-axis shows mass-to-charge (m/z) and X-axis shows retention time (minutes) from LC-MS from THP-1 cells. Upper panel shows species detected in positive ion mode, lower panel shows species detected in negative ion mode. **D**. Pie graphs showing the number of different lipid species arranged as lipid classes in THP-1 cells in both positive ion mode (left) and negative ion mode (right). Acar, Acylcarnitine, Cer, ceramide, Chol, cholesterol, DG, diacylglycerol, lysoPE, lysophosphatidylethanolamine, LPC, lysophosphatidylcholine, MG, monoacylglycerolipids, PA, phosphatidic acid, PC, phosphatidylcholine, PE, phosphatidylethanolamine, PE-NMe, monomethylphosphatidylethanolamine, PG, phosphatidylglycerol, PI, phosphatidyl inositol, PS, phosphatidylserine, SM, sphingomyelin, S-1P, sphingosine-1 phosphate, TAG, triacylglycerol. **E**. Heat-map showing clustering of mIDH1 AML and mIDH2 AML samples and normal CD34+ cells based on polar metabolites only. No separation between mIDH1 and mIDH2 is apparent and CD34+ cells cluster away from IDH mutants. **F**. Volcano plot showing fold change between all metabolites (polar + non-polar) in CD34+ vs mIDH2 AML. Dashed line represents unadjusted *P*-value of 0.01. **G**. Similar plot showing fold change between all metabolites (polar + non-polar) in CD34+ vs IDH1/2 wildtype AML. **H**. Volcano plot showing fold change AML wildtype and mIDH1. **I**. Volcano plot showing fold change between all metabolites (polar + non-polar) in wild type AML vs mIDH2 AML.

Supplementary Figure 2 (continued)

E

Polar Metabolites

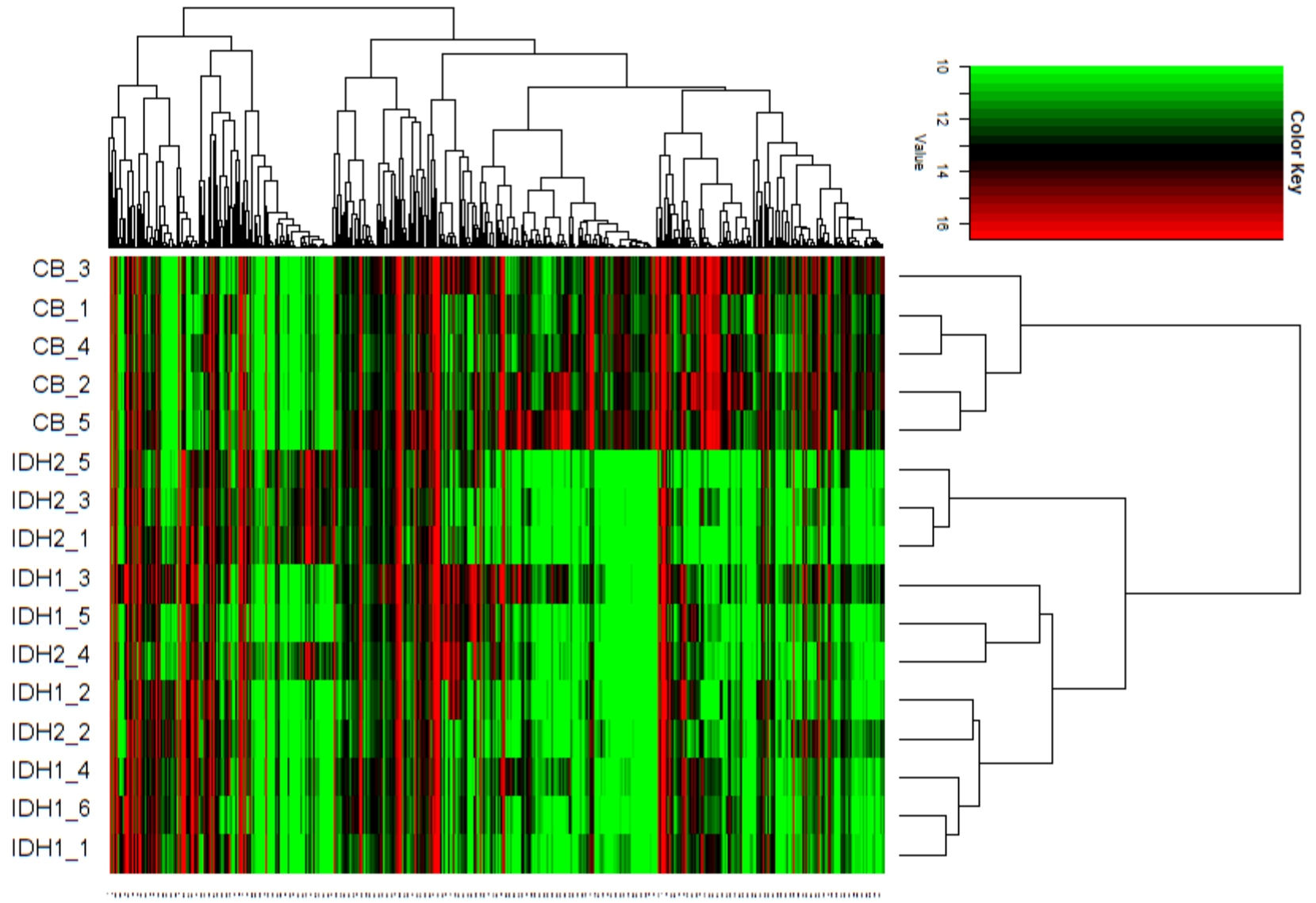

F

CD34+ vs mIDH2

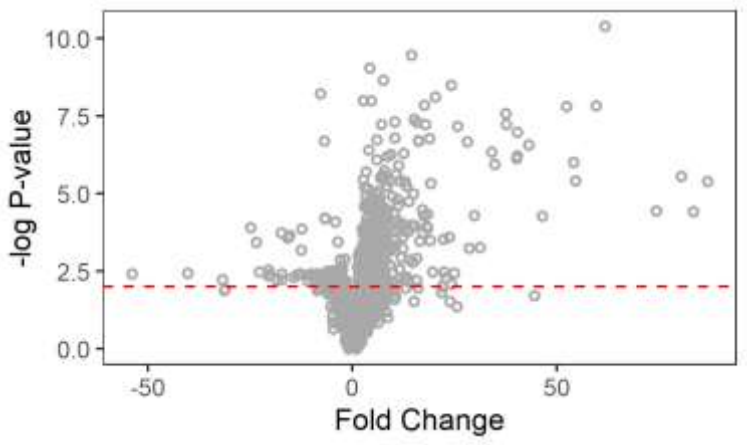

G

CD34+ vs AML WT

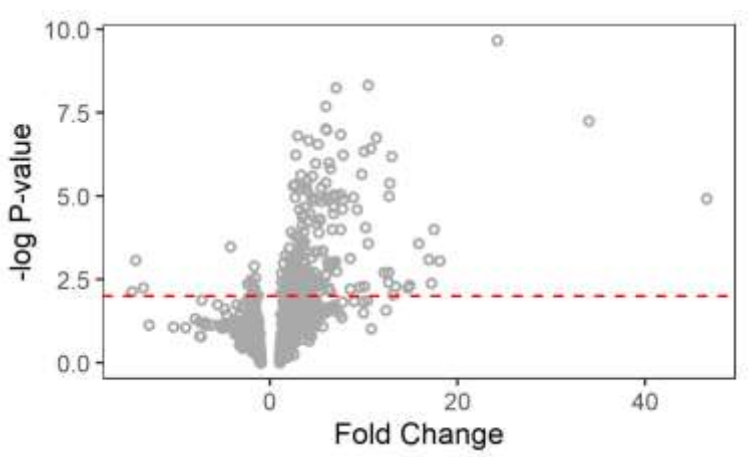

H

1°AML WT vs mIDH1

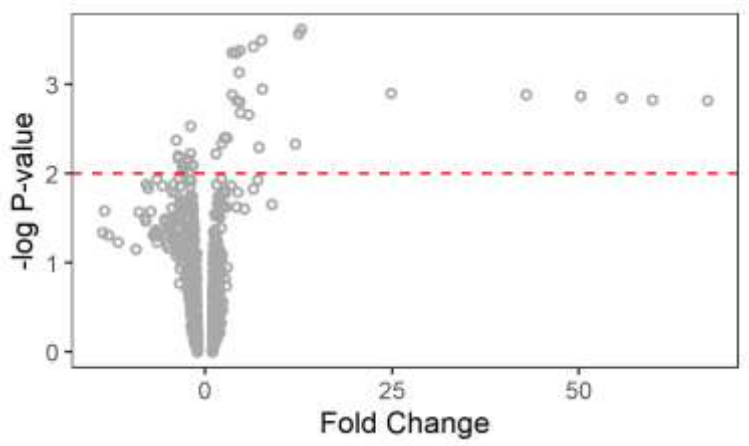

I

1°AML WT vs mIDH2

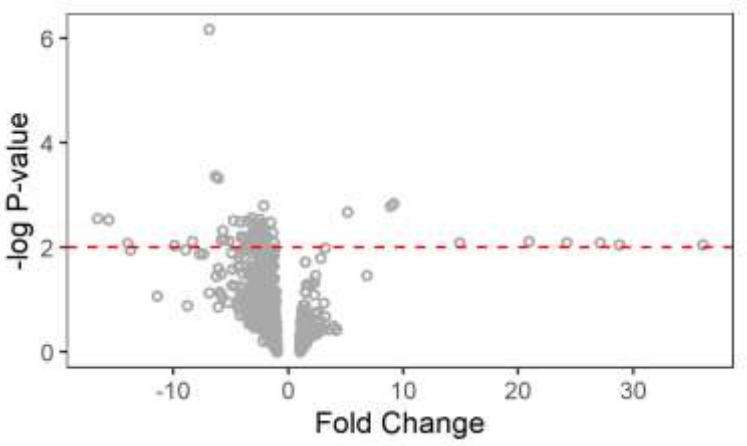

Supplementary Figure 3. Differences in metabolic flux observed between IDH1 and mIDH2 AML. A. Flux studies showing percentage of unlabelled M0 glycerol-3-phosphate derived from $^{13}C_{[1,2]}$ labelled glucose (2 of 6 carbons as heavy isotope) across isogenic THP-1 cells induced to express mIDH1 vs IDH1 wild type vs mIDH2 vs IDH2 wild type; same experiment as Figure 3B. **B**. Pentose phosphate pathway flux studies showing ribose M1 and M2 isotopologs from $^{13}C_{[1,2]}$ labelled glucose in THP-1 cells induced to express WT IDH1, mIDH1, IDH2 WT and mIDH2. No unlabelled (M0) ribose observed indicating all ribose derived from isotope-labelled glucose with *P* values for student's t-test as shown. **C**. Pentose phosphate pathway flux in primary AML. Flux studies showing ribose M1 and M2 isotopologs from $^{13}C_{[1,2]}$ labelled glucose mIDH1 vs mIDH2 AML. Complete incorporation of glucose into both oxidative and non-oxidative pentose phosphate pathways is observed in all samples. **D.** Column graphs showing abundance of Kreb's cycle metabolites from purified mIDH1 and mIDH2 primary blasts compared to normal cord blood CD34+ cells and IDH wild type AML. Bars represent standard error across 6 independent samples. All P values are Student's 2-tailed unpaired t-test compared with CD34+ unless otherwise shown. **E**. Flux studies showing unlabelled M0-citrate isotopolog derived from labelled glutamine across isogenic THP-1 cells induced to express mIDH1 vs IDH1 wild type vs mIDH2. No difference in unlabeled M0 isotopolog was noted between mIDH1 and wild type. Labelled glutamine was added to media in 2% hypoxia over 16 hours. Last column shows mIDH1 cells cultured in presence of 10 μM ivosidenib. This experiment was performed with 6 cell pellets for each sample blinded and randomised on mass spectrometry run. **F.** Same experiment showing percentage of labelled M4 citrate isotopolog, presumably derived from incorporation of U-$^{13}C_5$ glutamine into TCA cycle. **G**. Decreased reductive carboxylation of mIDH2 compared to IDH2 wild type +/- enasidenib in THP-1 cells measured by the percentage of M5 citrate isotopolog obtained from U-$^{13}C_5$ glutamine labeling in similar conditions to Figure 3A. This experiment was performed with 6 cell pellets for each sample blinded and randomized on each LC-MS run, *P<0.05, ** P<0.01, Student's t-test. **H**. Column graphs showing mean cell growth at 4 days after seeding mIDH1 (middle) vs isogenic WT HT-1080 cells (left panel) in lipid-deplete media with increasing concentrations of sodium acetate: 0, 0.1, 0.5 and 1 mM. Y-axis represents fold change acetate:H_2O of live cells measured by count beads. Bars represent averages of 3 independent experiments. Right panel shows mIDH1 cells pre-treated with 10 μM ivosidenib with increasing concentrations of acetate. Further details of wildtype revertants provided in Supplementary Figure 5. **I**. Western blot showing equivalent levels of acetate substrate enzyme acetyl-CoA synthetase across WT, mIDH1 and mIDH1+ivosidenib treated cells in previous experiment. **J**. Acylcarnitine abundance in THP-1 cells induced with mIDH1 (+dox) vs endogenous wild type (-dox) (top panel) or THP-1 cells induced with mIDH2 (+ dox) vs wildtype (- dox) measured by LC-MS in positive ion mode on C18 column. Y-axis represents the number of molecules. **K**. Representative examples of oxygen consumption and the etomoxir-inhibitable component in wild-type vs mIDH1 representing endogenous fatty acid oxidation. **L**. Graph showing ratio of reduced NADPH to total NADP(H) from primary genotyped patient samples; same experiment as Figure 3C. ANOVA did not reveal statistical differences between groups. **M-O**. Relative abundance of reduced and oxidised glutathione measured in individual mIDH1 and mIDH2 primary AML as measured by mass spectrometry. Bars represent standard deviations of 3 technical replicates per patient sample, total n=4. In **O**, bars represent standard error of mean, *P* = not significant, Student's t-test.

Supplementary Figure 3

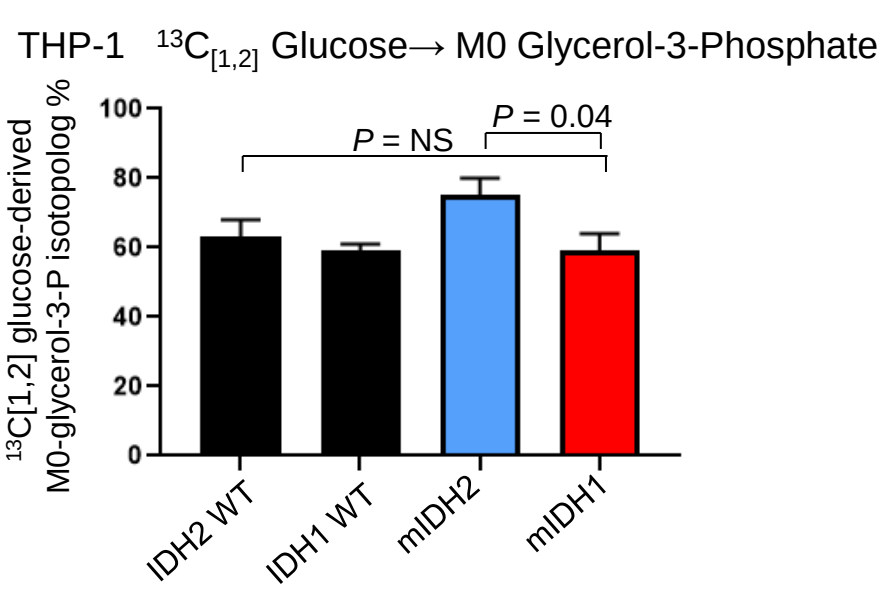

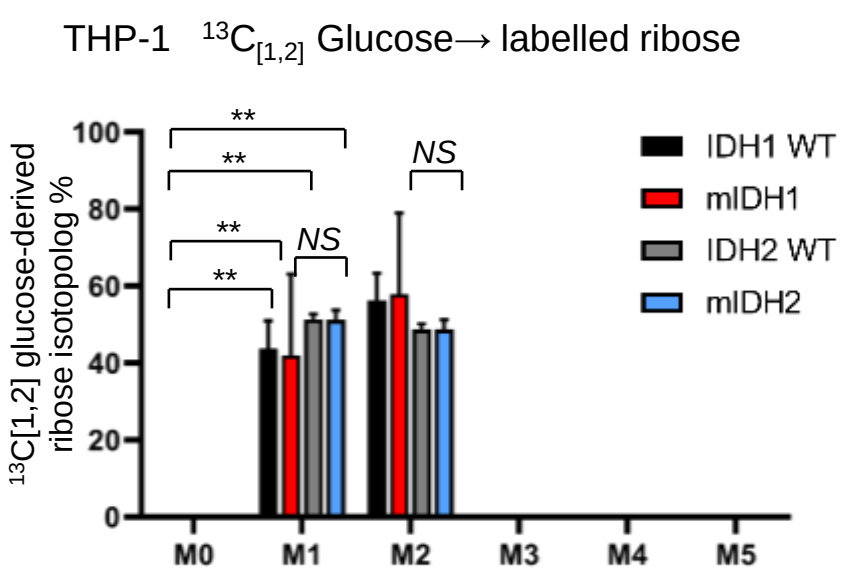

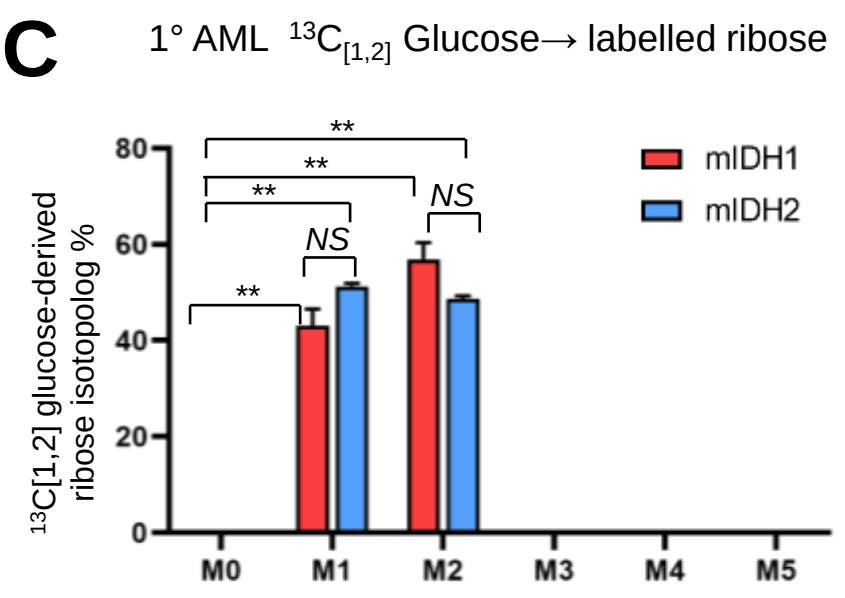

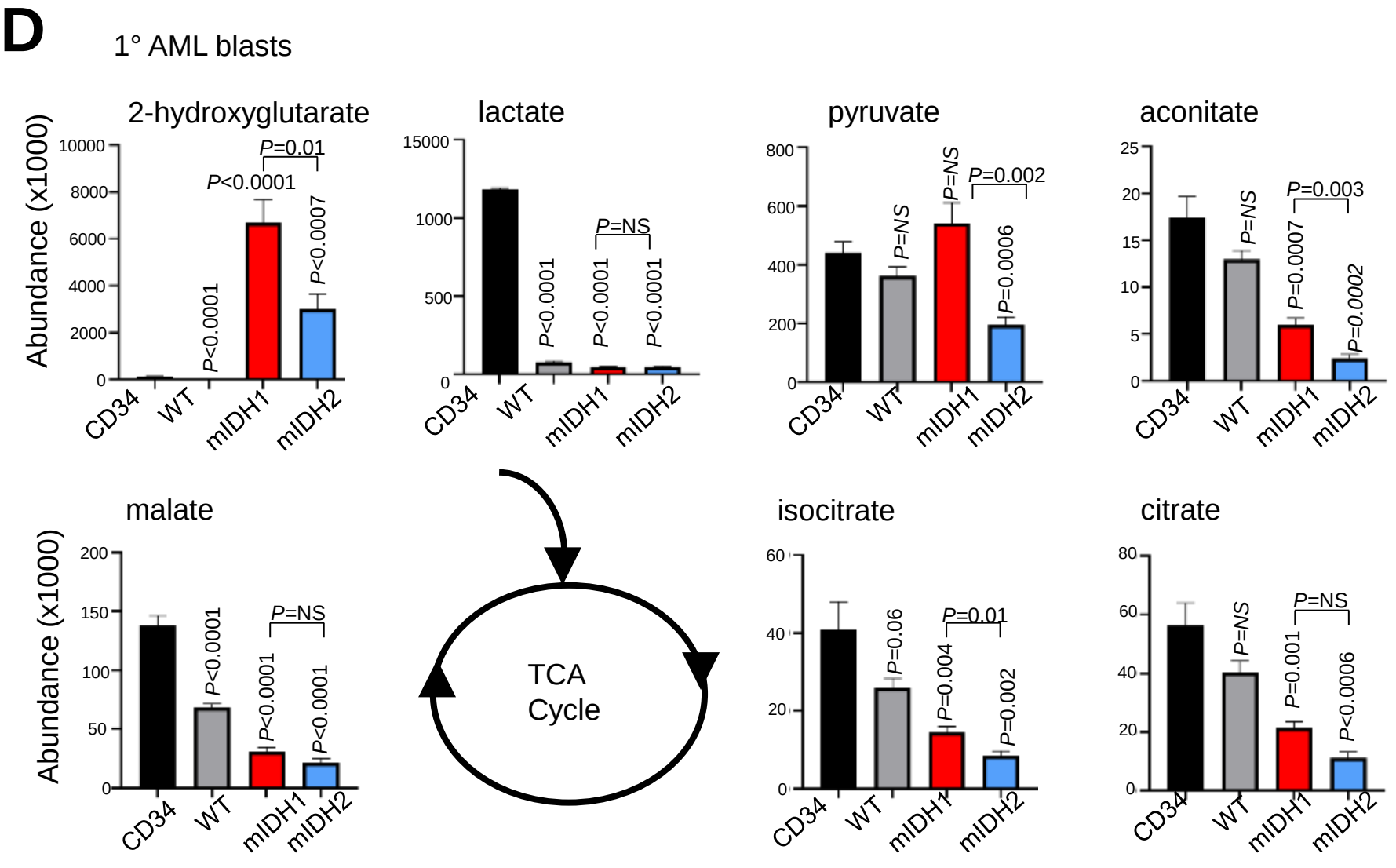

Supplementary Figure 3 (continued)

E

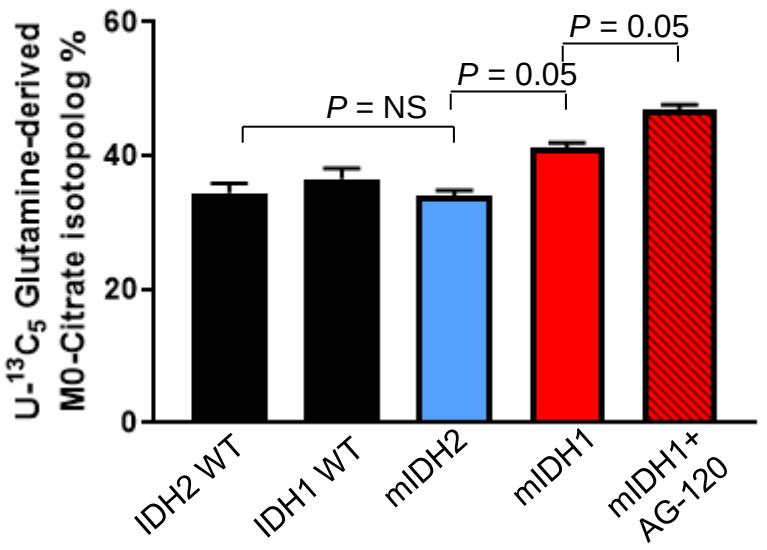

F

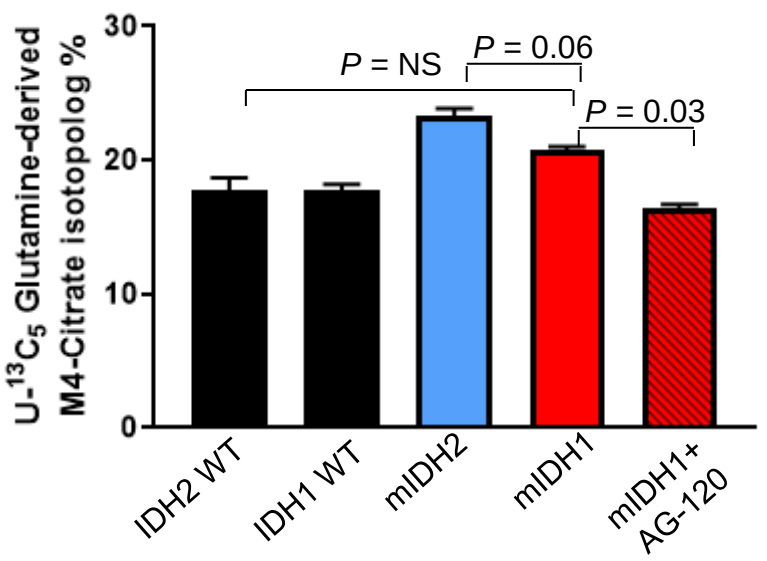

G

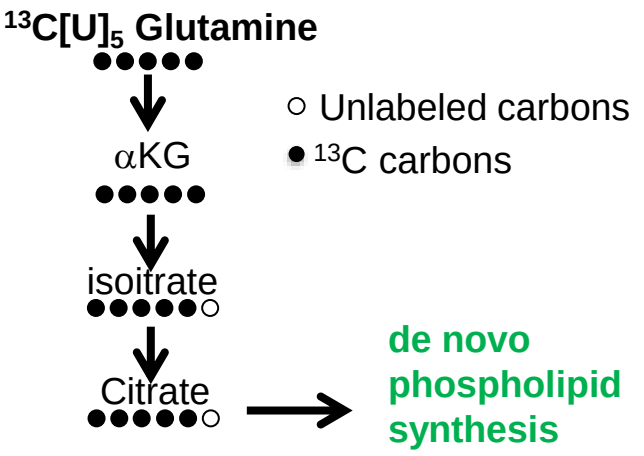

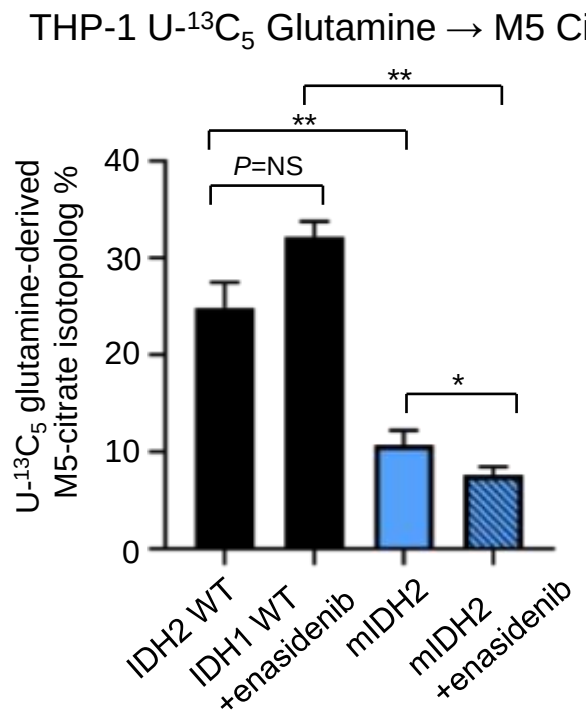

H

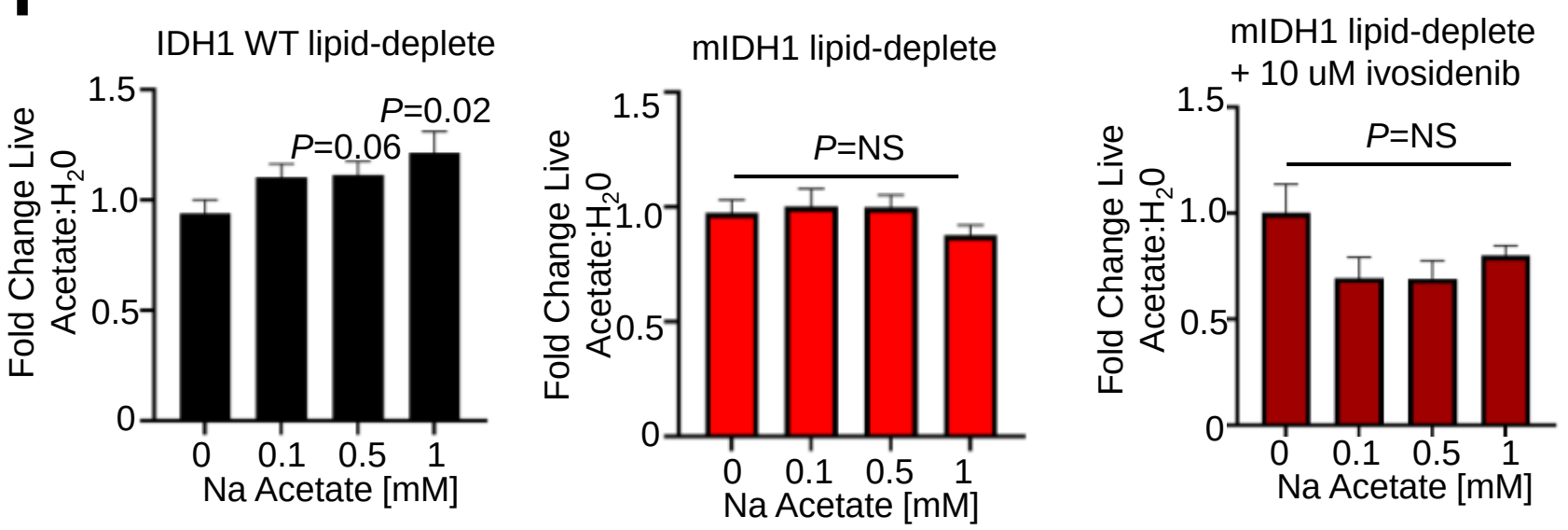

I

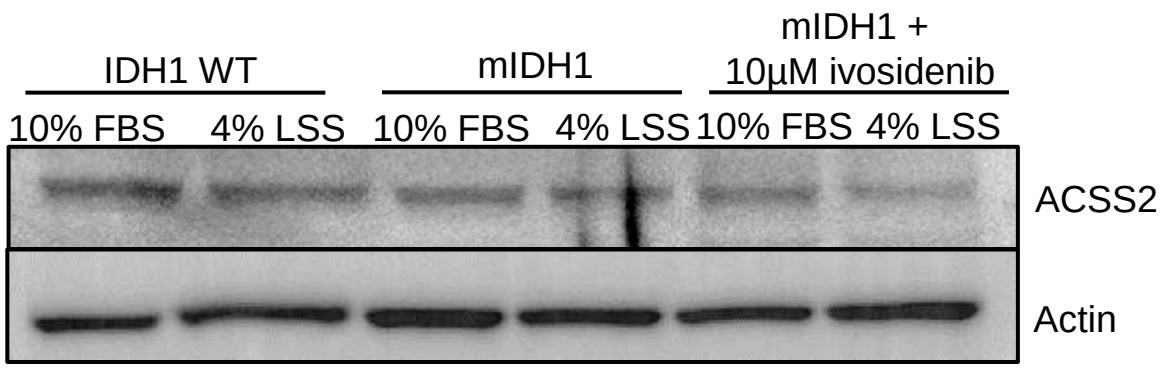

Supplementary Figure 3 (continued)

J

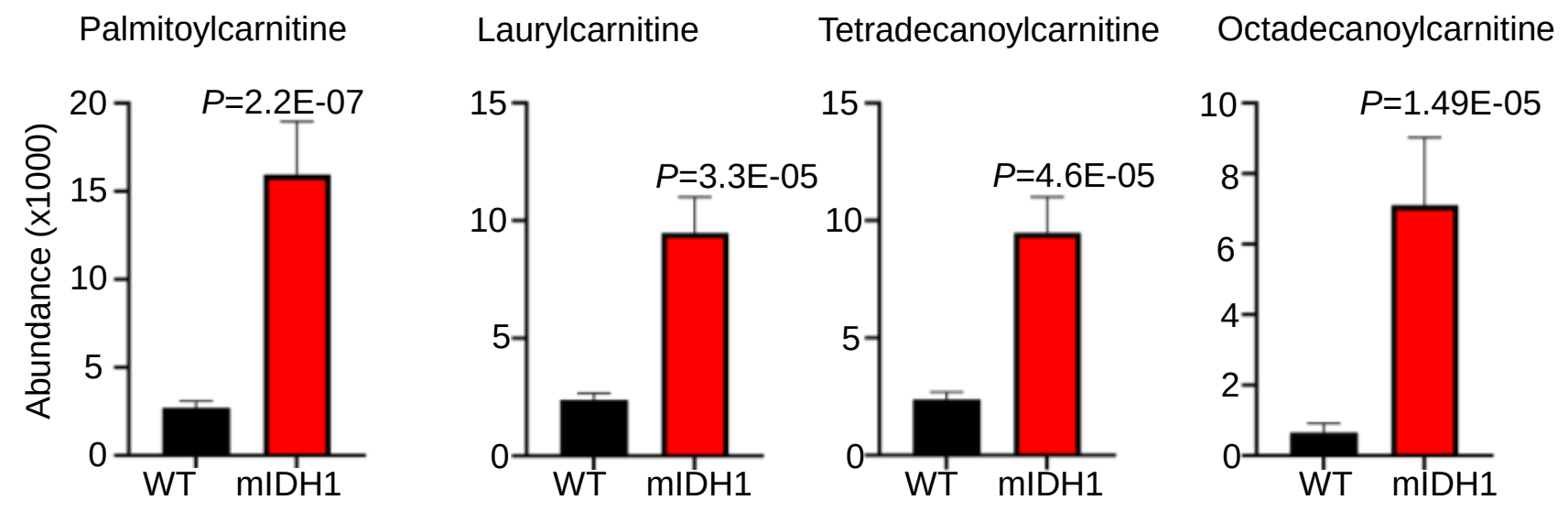

K

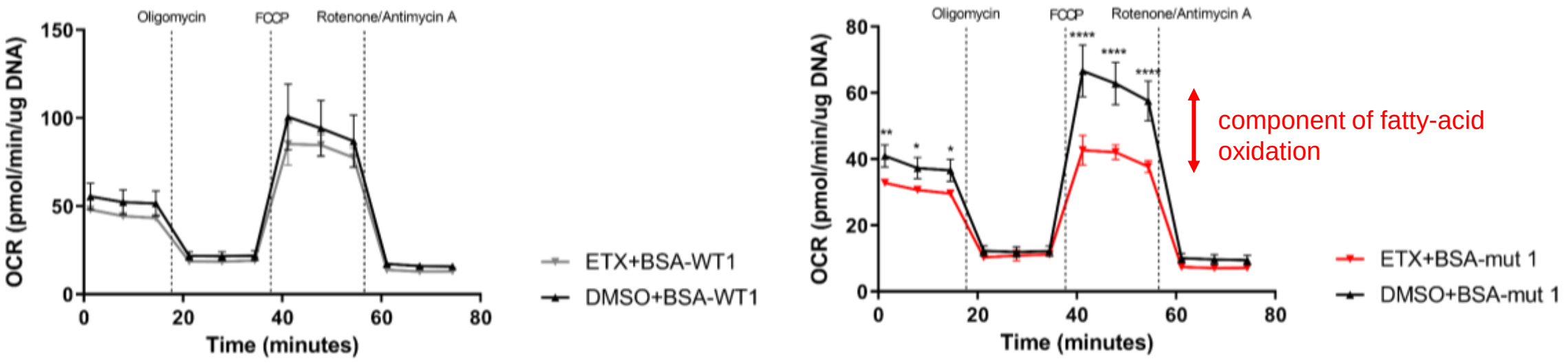

Supplementary Figure 3 (continued)

L

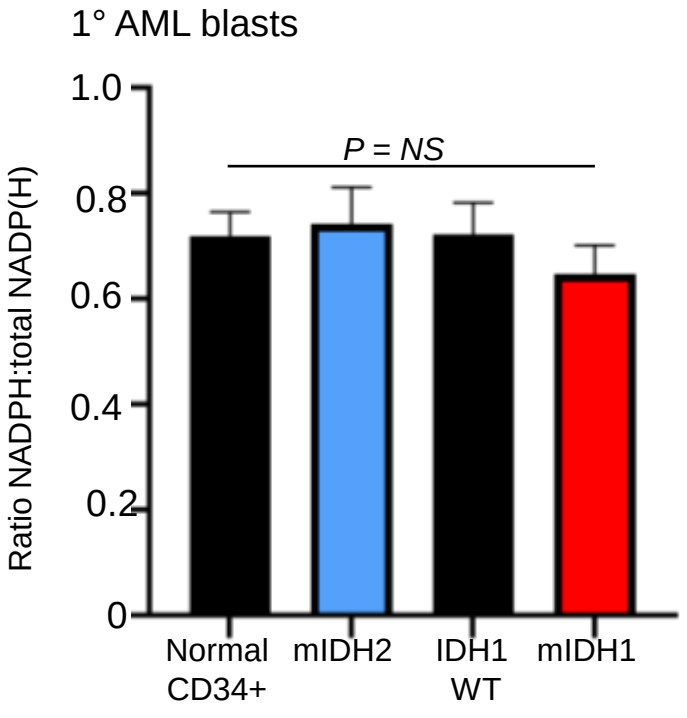

M 1° AML

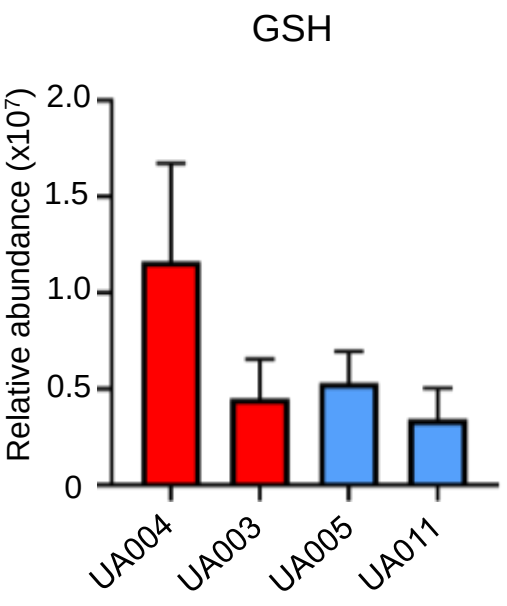

N 1° AML

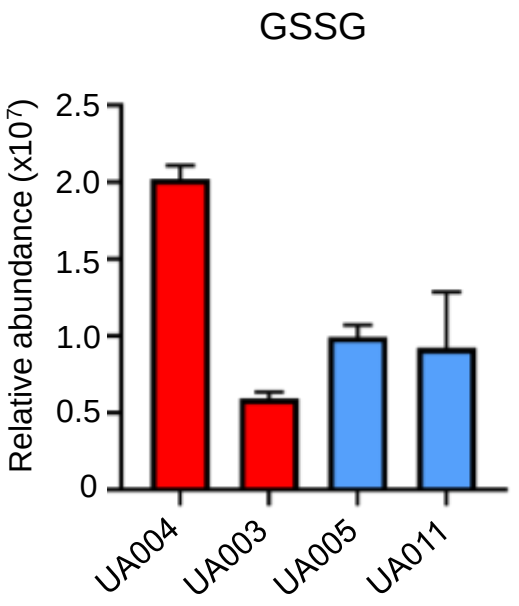

O 1° AML

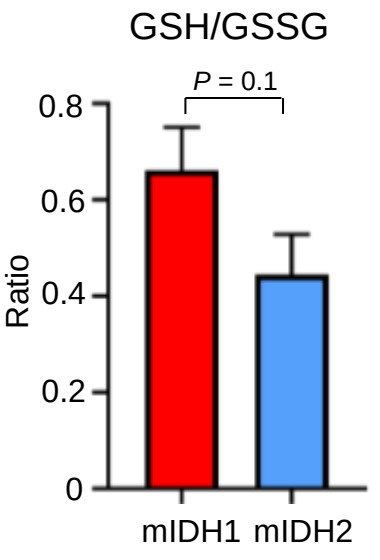

Supplementary Figure 4

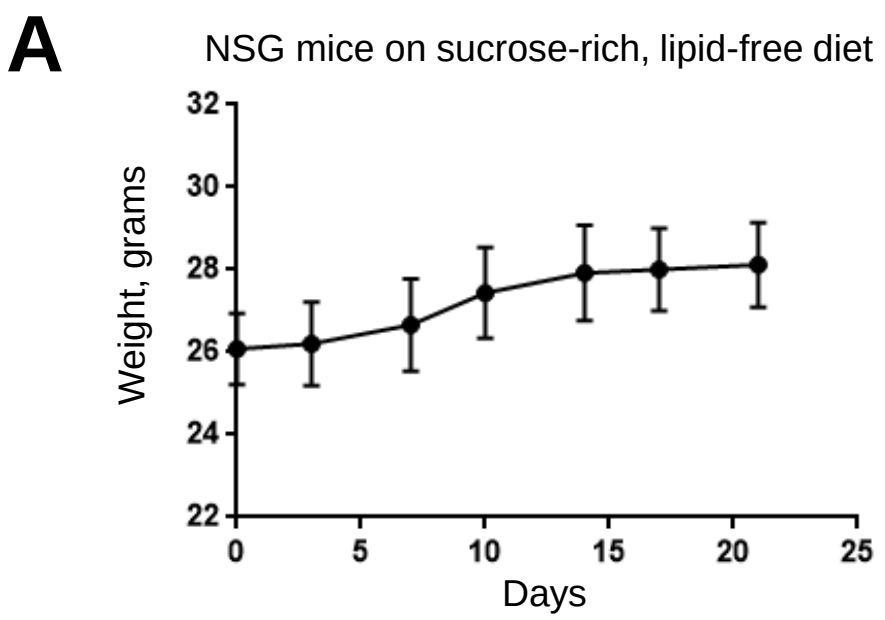

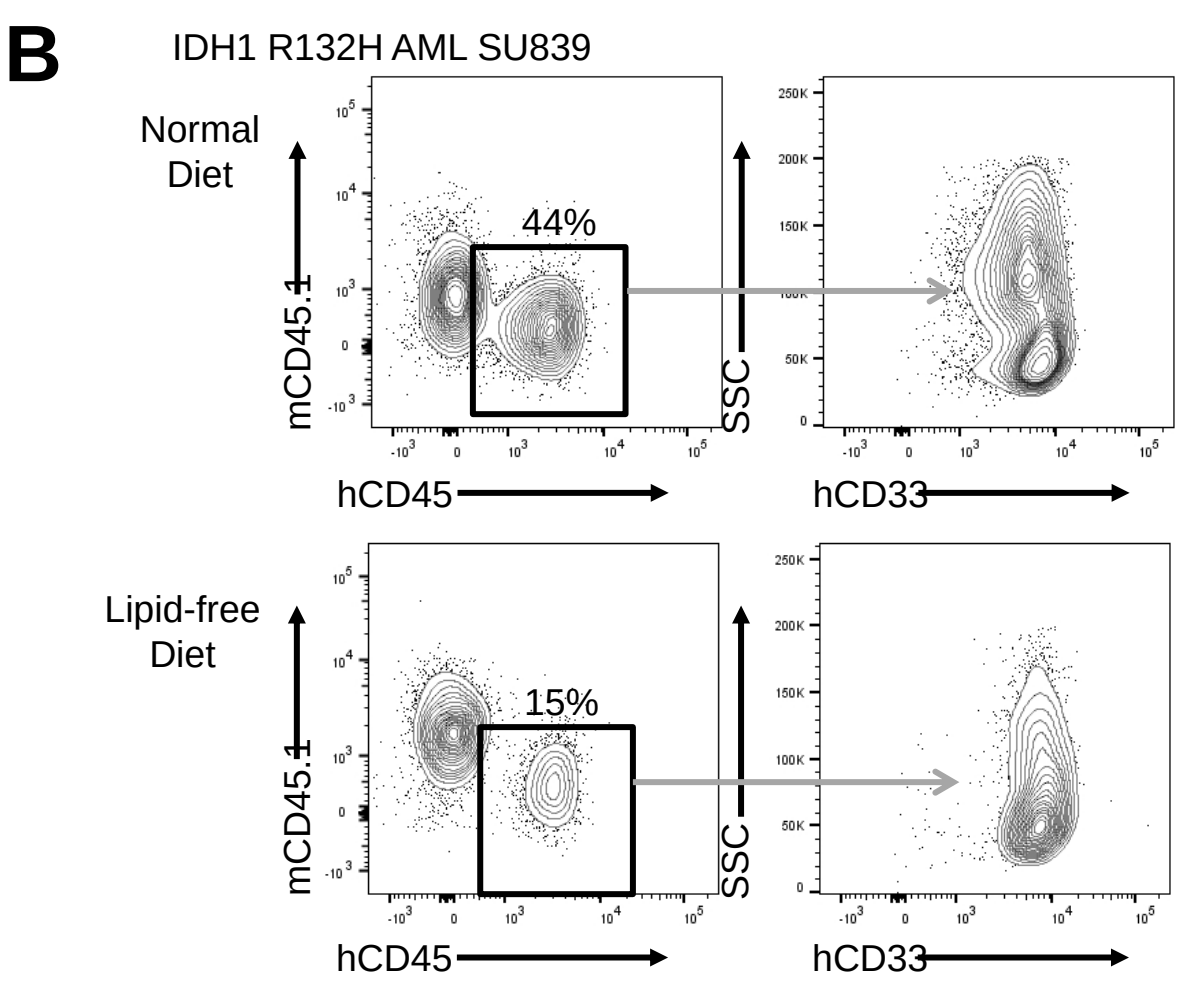

Supplementary Figure 4. Mice continue to maintain weight on lipid-free diet. A. NSG mice (n = 10) fed on sucrose-rich lipid free diet at a minimum of 4 weeks after weaning continued to gain weight. **B.** Representative flow plots showing decreased engraftment of CD33+hCD45+ AML after 6 weeks on lipid-free diet compared with normal diet.

Supplementary Figure 5

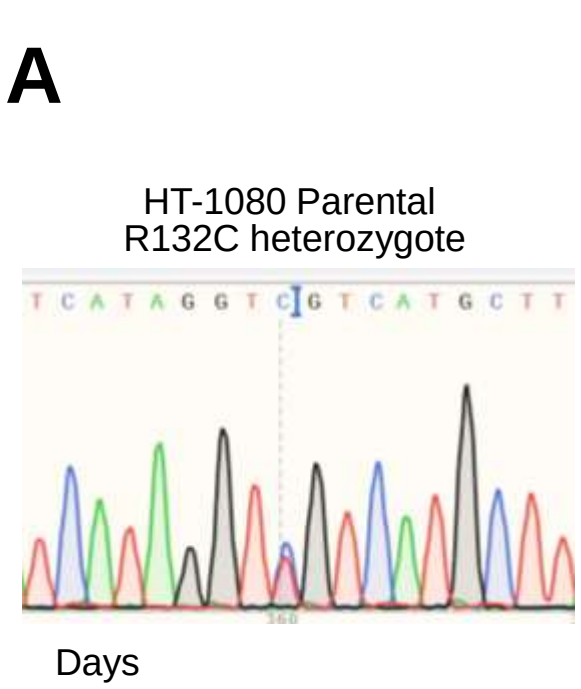

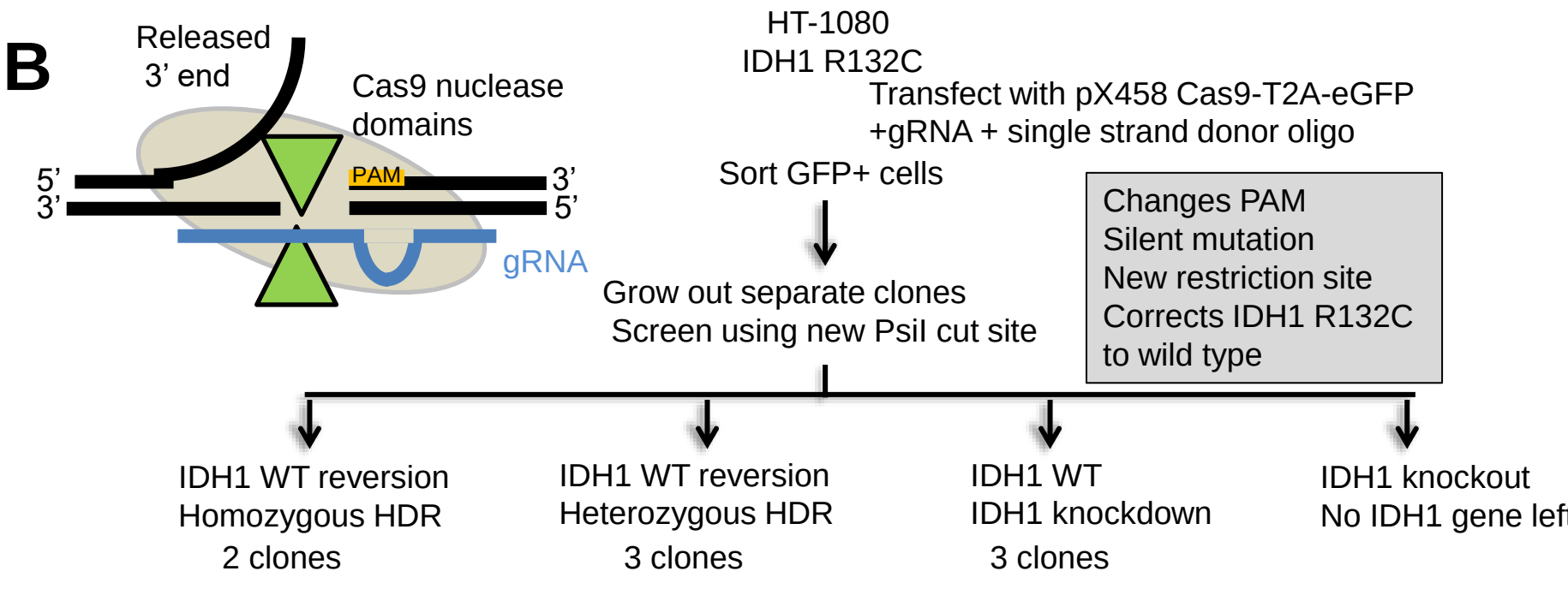

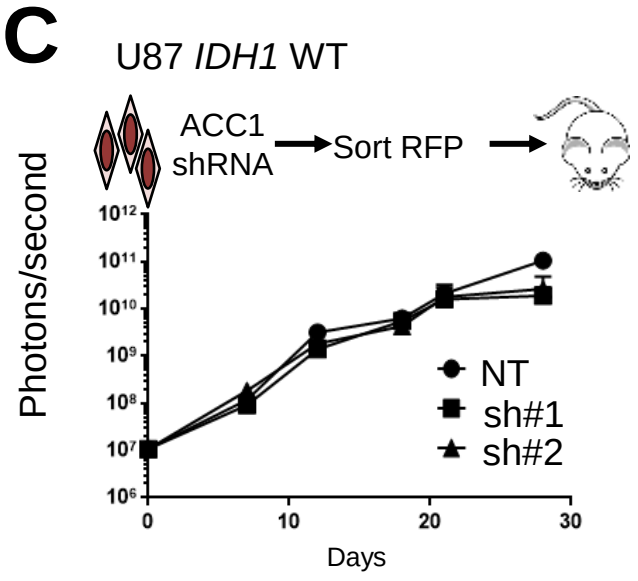

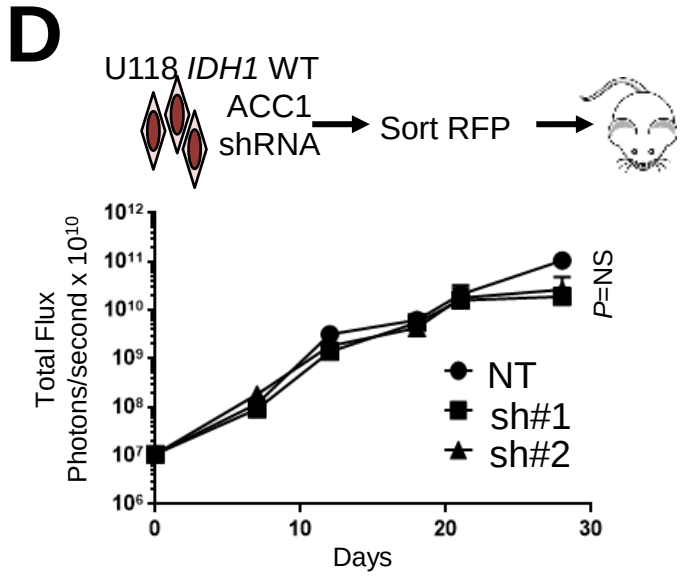

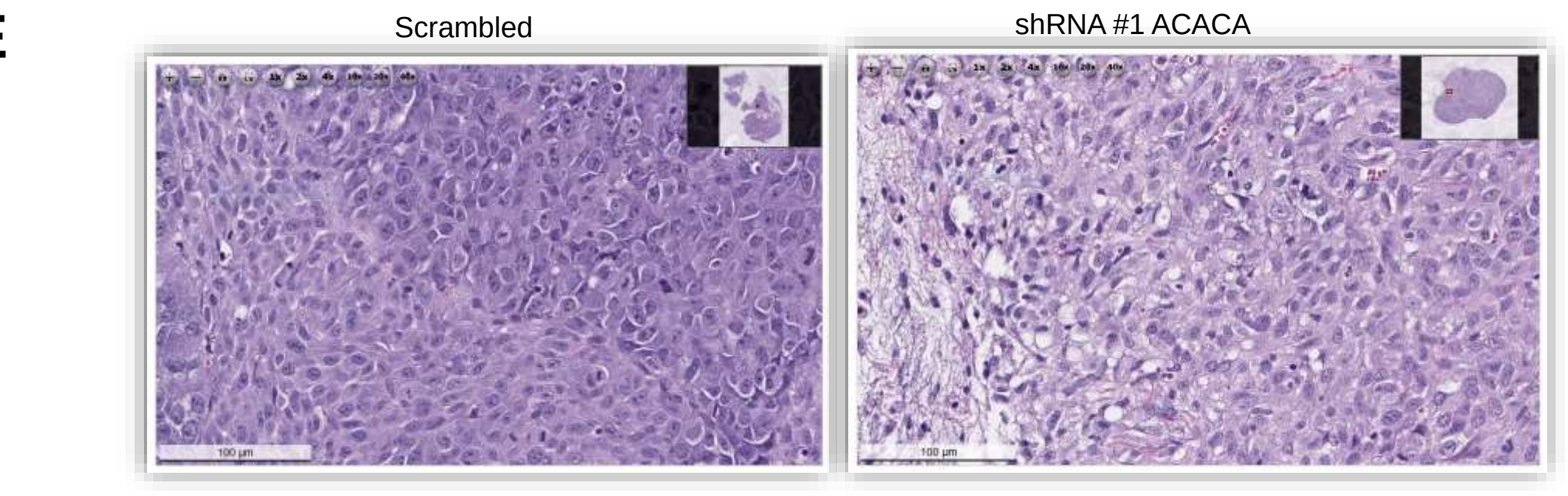

Supplementary Figure 5. Targeting ACC1 in IDH1 wild type cells. A. Validation of heterozygous IDH1 mutation in parental HT-1080 by Sanger sequencing. **B**. Schematic showing method to induce *IDH1* wild type reverted cells using transfected pX458 Cas9-T2A-eGF + gRNA + single strand donor oligo by introduction of a silent mutation that disrupts PAM sequence, introduces silent mutation and a new restriction PsiI cut site for rapid screening. **C**.. In vivo growth of U87 IDH1 wild-type cell line transplanted into flank of NSG mice over 30 days after ACC1 knockdown or non-targeting control. **D.** In vivo growth of U118 IDH1 wild-type cell line transplanted into flank of NSG mice over 30 days after ACC1 knockdown or non-targeting control. **E.** Histology (hematoxylin and eosin stain) of tumor explants in ACC1 knockdown tumors compared to non-targeting controls.

Supplementary Figure 6

Supplementary Figure 6. Targeting ACC1 with small molecule inhibitors. A. TOFA dose response curves with calculated IC_{50} shown for IDH1 wild type U87 glioblastoma cells transduced with either IDH1 wild type or IDH1 R132H mutation. The number of DAPI-negative cells grown in 0.5% serum was determined by flow cytometry 72 hours after addition of drug. **B,C**. Decreased lysophospholipids, LPC = lysophosphatidylcholine, LPE = lysophosphatidylethanolamine in mIDH1 HT-1080 vs wildtype revertants measured by LC-MS, lipid-depleted conditions. **D**. Western blot showing PRKA1 shRNA knockdown in HT-1080 wild type and mIDH1 growing in lipid replete conditions. Note basal pACC1 reduced in mIDH1 cells compared to wild type. **E**. Rescue of mIDH1 growth over 4 days in lipid-deplete conditions after PRKA1 knockdown or AMPK inhibitor dorsomorphin. **F**. THP-1 R132H cells treated with 10 μM TOFA +/- 10 μM ivosidenib. **G**. Change in weight over time after TOFA or vehicle administration in PDx mice for 30 days.

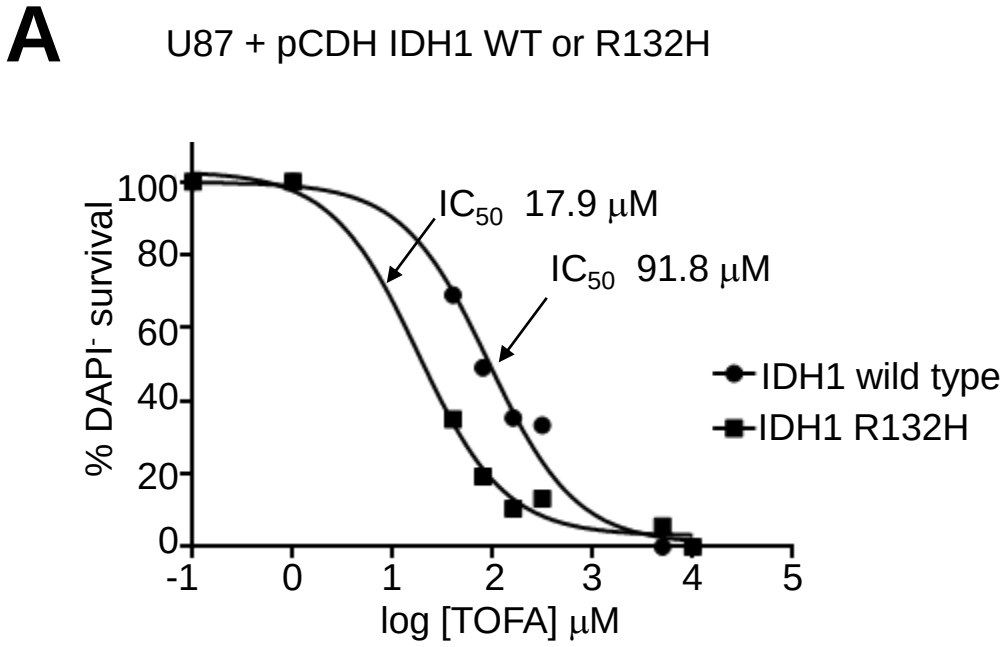

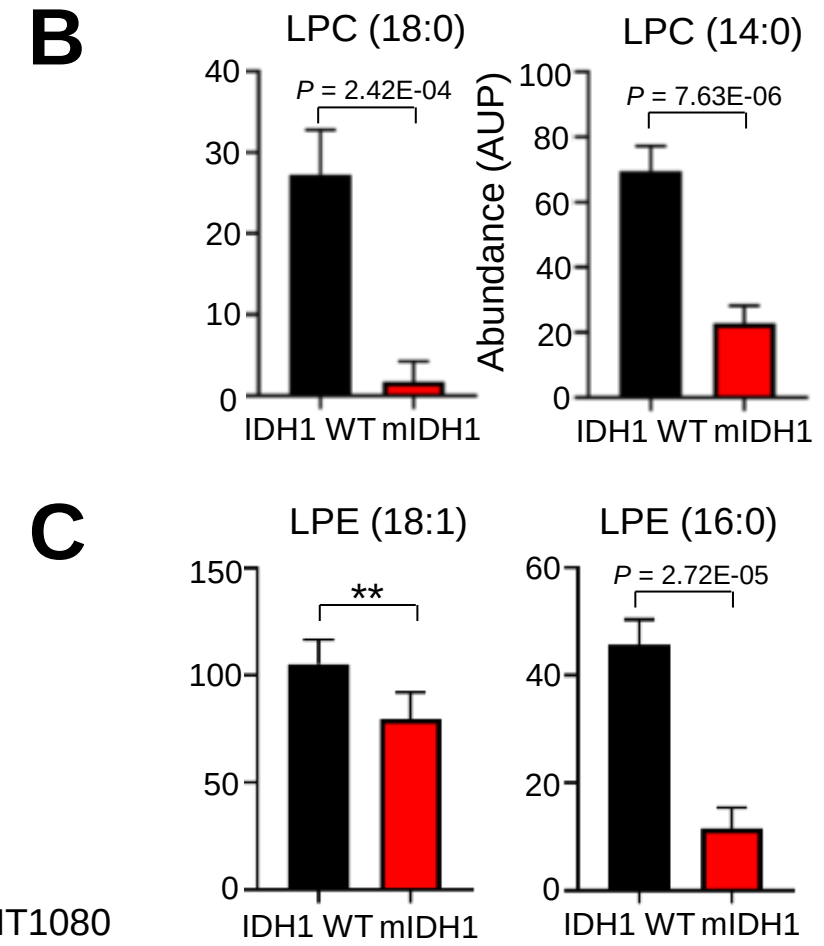

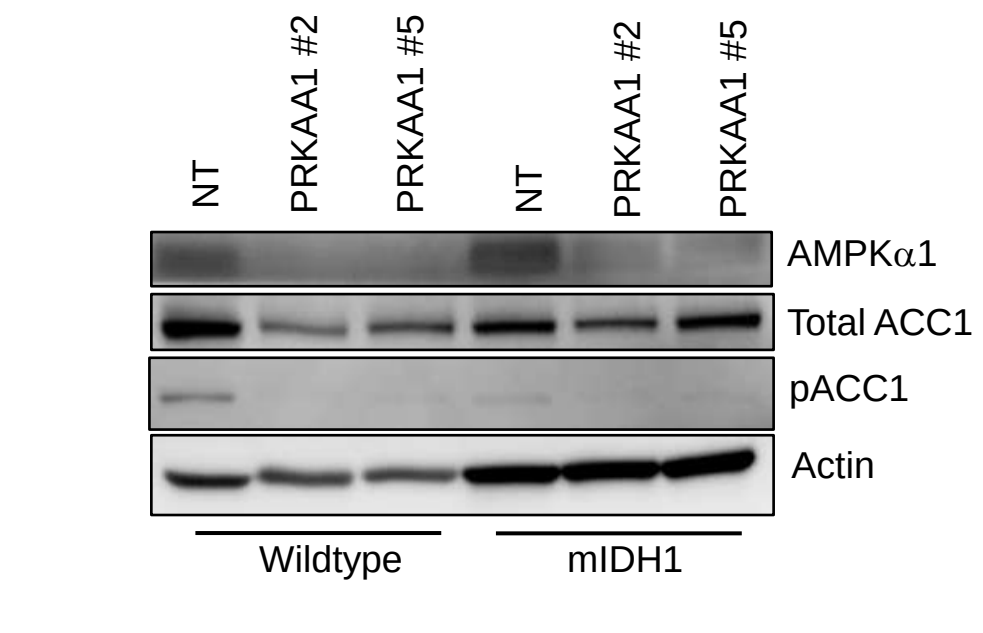

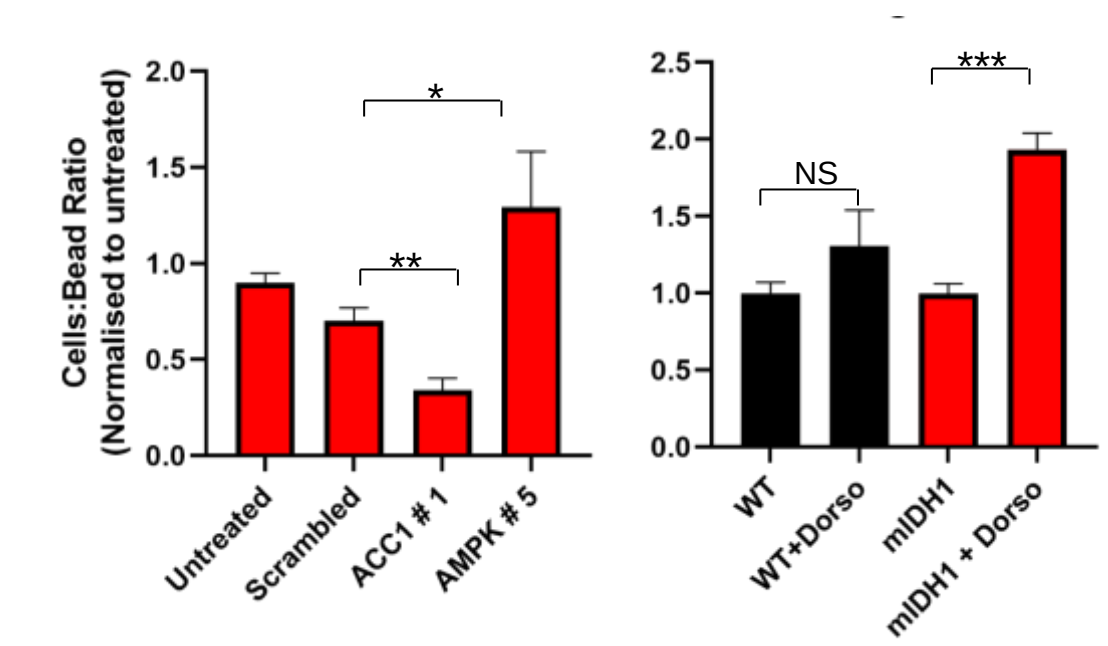

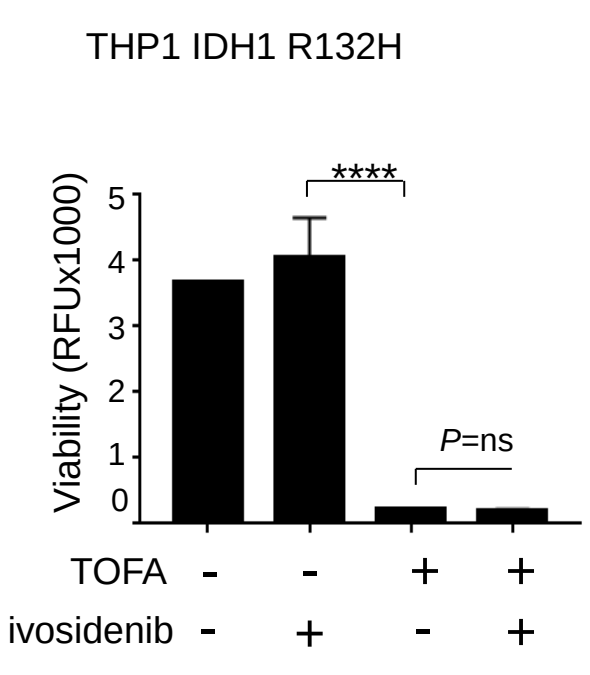

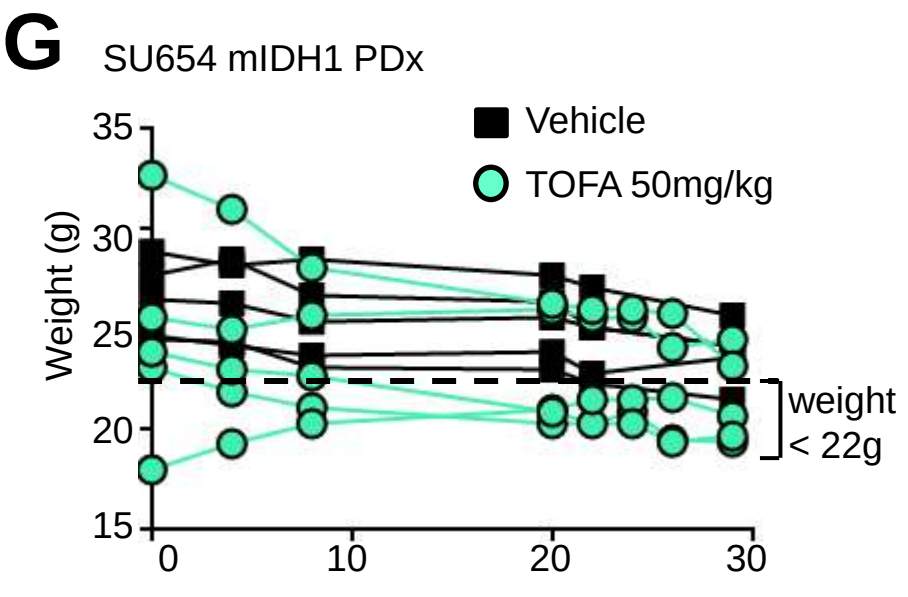

Supplementary Figure 7

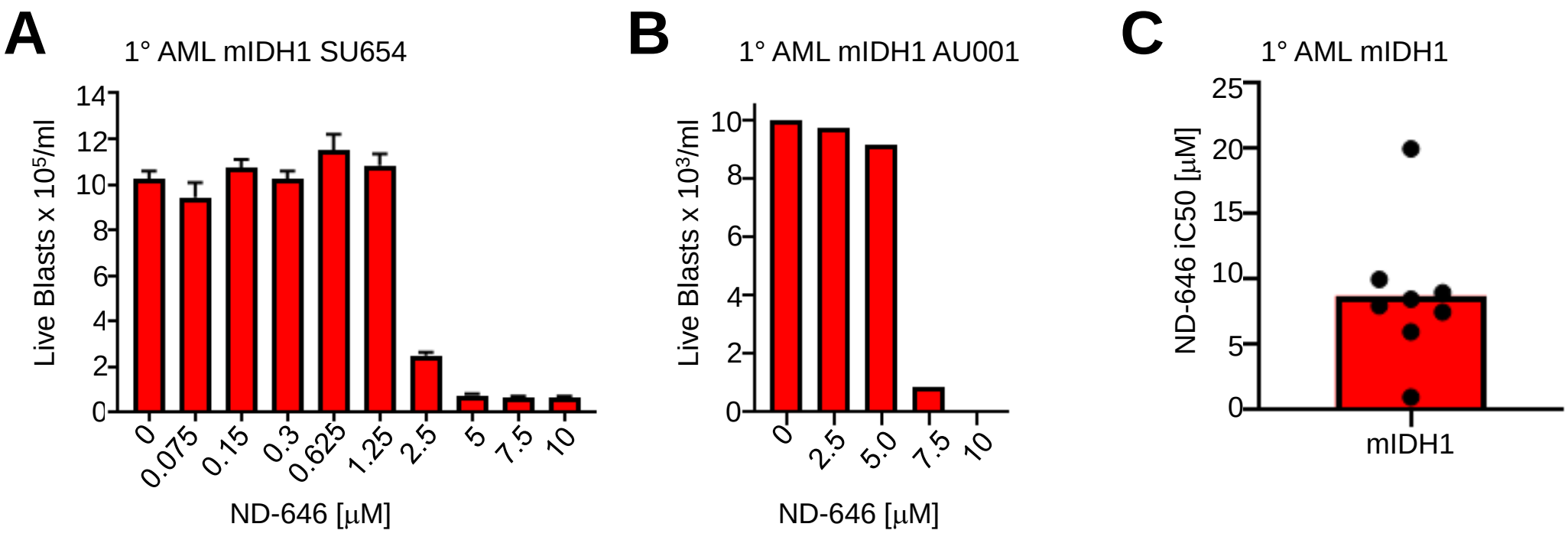

Supplementary Figure 7. ND-646 overcomes venetoclax resistance. A, B. Low micromolar concentrations of ND-646 have activity blocking growth of primary mIDH1 AML blasts over 72 hours in 0.5% lipid-stripped IMDM with myeloid growth factors. Primary mIDH1 AML blasts were purified from dead cells, T-cells and B-cells using magnetic bead selection and treated with increasing concentration of ACC1/ACC2 dual inhibitor ND-646 with the concentrations indicated. The number of live DAPI-negative blasts was measured relative to fluorescent tru-count beads by flow cytometry. Bars represent standard deviation of technical replicates for each dose. **C**. Graph summarizing average ND-646 IC50 mM for mIDH1 AML. D. Schematic for inducing resistance to 100 nM ABT-199 in THP-1 IDH1 R132H cells by increasing concentration by 2 nM every 3 days, starting at 5 nM. **E**. THP-1 IDH1 R132H cells (ABT-199 naïve) treated with 10 μM TOFA or 50 nM ABT-199 in lipid-replete media. **F**. THP-1 ABT-199-resistant cells IDH1 R132H cells treated with 10 μM TOFA or 50 nM ABT-199 for 72 hours in lipid-replete media. Bars represent standard error for 3 independent experiments, *P* = Student's t-test. **G**. Minimal weight change over time during oral gavage treatment with vehicle, ABT-199 or combination therapy..